Potentiation of 5-fluorouracil encapsulated in zeolites as drug delivery systems for *in vitro* models of colorectal carcinoma

Natália Vilaça,[a] Ricardo Amorim,[b,c] Ana F. Machado,[a] Pier Parpot,[a] Manuel F.R. Pereira,[d] Mariana Sardo,[e] João Rocha,[e] António M. Fonseca,[a] Isabel C. Neves*[a] and Fátima Baltazar*[b,c]

[a]*Centre of Chemistry, Chemistry Department, University of Minho, Campus de Gualtar, 4710-057 Braga, Portugal - E-mail: (ineves@quimica.uminho.pt)*

[b]*Life and Health Sciences Research Institute (ICVS), School of Health Sciences, University of Minho, Campus Gualtar, Braga, Portugal - E-mail: (fbaltazar@ecsaude.uminho.pt)*

[c]*ICVS/3B's - PT Government Associate Laboratory, Braga/Guimarães, Portugal*

[d]*Laboratory of Catalysis and Materials (LCM), Associate Laboratory LSRE/LCM, Faculdade de Engenharia, Universidade do Porto, Rua Dr. Roberto Frias, 4200-465 Porto, Portugal*

[e]*CICECO – Chemistry Department, University of Aveiro, Campus de Santiago, 3810-193 Aveiro, Portugal*

ABSTRACT

The studies of potentiation of 5-fluorouracil (5-FU), a traditional drug used in the treatment of several cancers, including colorectal (CRC), were carried out with zeolites Faujasite in the sodium form, with different particle sizes (NaY, 700 nm and nanoNaY, 150 nm) and Linde type L in the potassium form (LTL) with a particle size of 80 nm. 5-FU was loaded into zeolites by liquid-phase adsorption. Characterization by spectroscopic techniques (FTIR, ^{1}H NMR and ^{13}C and ^{27}Al solid-state MAS NMR), chemical analysis, thermal analysis (TGA), nitrogen adsorption isotherms and scanning electron microscopy (SEM), demonstrated the

successful loading of 5-FU into the zeolite hosts. *In vitro* drug release studies (PBS buffer pH 7.4, 37 ºC) revealed the release of 80-90% of 5-FU in the first 10 min. To ascertain the drug release kinetics, the release profiles were fitted to zero-order, first-order, Higuchi, Hixson-Crowell, Korsmeyer-Peppas and Weibull kinetic models. The *in vitro* dissolution from the drug delivery systems (DDS) was explained by the Weibull model. The DDS efficacy was evaluated using two human colorectal carcinoma cell lines, HCT-15 and RKO. Unloaded zeolites presented no toxicity to both cancer cells, while all DDS allowed an important potentiation of the 5-FU effect on the cell viability. Immunofluorescence studies provided evidence for zeolite-cell internalization.

Keywords: Zeolites; 5-fluorouracil (5-FU); encapsulation; drug delivery; cytotoxicity; potentiation

1. Introduction

Colorectal carcinoma (CRC) is one of the most common types of cancer in industrialized countries, slightly more prevalent in men than women [1]. Generally, the treatment of CRC includes surgery, radiotherapy and/or chemotherapy. The treatment design depends, however, largely on the cancer stage. Although for patients with an early-stage disease, surgery gives a relatively good prognosis; patients in a more advanced disease stage often require adjuvant chemotherapy to reduce cancer and the high risk of recurrence [2-4].

5-Fluorouracil (5-FU) has been in use for about 50 years [5], being one of the most effective chemotherapeutic agents in the treatment of CRC, stomach, breast, and head & neck cancers [6,7]. Despite the progress made with the introduction of new cytotoxic agents and medical practices, the survival rates of CRC patients changed little over the past 20 years [8-12], justifying the need for more effective therapies.

Therapy with classical drugs such as 5-FU, has important toxic side effects. Thus, encapsulation in sustained delivery systems may contribute to reduce these side effects and maybe allow oral administration. 5-FU is administered intravenously due to its variable gastrointestinal absorption and rapid degradation [13,14]. There are several advantages to oral drug administration, including patient's convenience and the reduced costs associated with drug preparation and administration [4]. The efficacy of 5-FU therapy may also be enhanced and its toxicity diminished by association with delivery systems that selectively convey this active agent while, at the same time, reduce its toxicity [15]. Moreover, encapsulation may allow drugs to be released in a controlled way to the cancer area, preventing degradation of the anticancer drug [4,15,16].

Several recent studies showed that the potential of zeolites in medical applications is due to their structural properties and stability in biological environments [17,18]. Zeolites have also been explored as suitable hosts for the encapsulation of drug molecules, in search for efficient DDS. Both zeolites and drugs have been administrated simultaneously to a patient without loss of the individual pharmacological effect of the drugs [17-28].

Zeolites are solid hydrated crystalline materials with frameworks comprising silicon, aluminum and oxygen and featuring nano-channels and cages of regular dimensions [29]. The pores of zeolites are open to the surrounding medium, thus allowing diffusion of molecules from the exterior to the interior of the zeolite particle. Zeolites exhibit a large specific surface area, typically in excess of 400 m^2 g^{-1}, with most of this area being internal (void volume above 0.10 cm^3 g^{-1}), and are very stable in different media [29]. The water molecules within the cavities are loosely bound and are easily removed upon heating, resulting in a high surface area and accessible pore volume [29].

In previous studies we have reported the preparation of DDS based on zeolite structures with the experimental anticancer drug α-cyano-4-hydroxycinnamic acid (CHC) and demonstrated its efficacy against colorectal carcinoma cells [30,31]. As a continuation of this line of

research, the anticancer drug 5-FU was encapsulated into two zeolites with diverse frameworks and particle size. Zeolite L is an aluminosilicate bearing parallel one-dimensional channels with pore openings of *ca.* 0.71 nm in diameter, able to host a large variety of small molecules [32]. Zeolite Y consists of supercages with a diameter of 1.18 nm, sharing a 12-membered ring with an aperture of 0.74 nm [33], suitable to accommodate various compounds [33-36]. These new DDS were characterized by a range of methods, spectroscopic techniques (FTIR and ^{13}C and ^{27}Al solid-state MAS NMR), scanning electron microscopy (SEM), thermogravimetric analysis (TGA), nitrogen adsorption isotherms and elemental analysis. The effect of zeolites and DDS was evaluated on HCT-15 and RKO human colon carcinoma cell viability. Zeolite-cell internalization was also assessed.

2. Materials and Methods

2.1. Materials

Linde Type L zeolite powder in the potassium form (NanoZeolite LTL, Si/Al = 3.40) with ~ 80 nm average particle size was purchased from NanoScape. Two faujasite zeolites with different particle sizes were commercially available in the sodium form and as a powder; NaY zeolite (Si/Al = 2.83, CBV100) was obtained from Zeolyst International and nanoNaY zeolite (NanoFAU-Y, Si/Al = 2.25) from NanoScape. 5-fluoro-1H-pyrimidine-2,4-dione usually know as 5-fluorouracil (5-FU) was used as obtained from Sigma-Aldrich (99%). Rhodamine B was supplied by Merck (≥90%).

2.2. Preparation of 5-FU@zeolites

Loading of 5-FU into zeolites was based on a previously established procedure [30,31]. Before 5-FU loading, the zeolite powders were dehydrated at 120 °C overnight in order to remove the water from the pores. 5-FU loading into the zeolites was achieved by mixing 100 mg of each zeolite with a solution of 5-FU (130 mg, 0.99 mmol) in acetone (15 mL) as a solvent and was stirred (300 rpm) for 48 h at room temperature. The mixture was filtered and

the resulting DDS dried in an oven at 60 ºC for 12 h. This temperature is enough to evaporate the acetone solvent. Throughout the manuscript, the obtained DDS will be referred to as 5-FU@zeolite, where zeolite represents the structure of the zeolite used. Also, preliminary studies with other solvents in which 5-FU is soluble (ethanol and methanol) were carried out under the same experimental conditions to which the 5-FU@zeolite samples were submitted. After preparation of the DDS, these solvents remained adsorbed in the zeolite structures and are toxic to the cell lines studied. The amount of loaded 5-FU was measured using thermogravimetric analysis (TGA). In order to evaluate the solvent effect, the zeolites were prepared with 15 mL of solvent, using the same experimental conditions as the DDS samples.

The cellular location of NaY was monitored by loading this zeolite with Rhodamine B. This compound was loaded into NaY by stirring (300 rpm, 48h at room temperature) a mixture of 100 mg of zeolite in a solution of Rhodamine B (20 mg, 0.042 mmoles) in acetone (15 mL). The reaction vessel was lined with foil to protect from light. The mixture was filtered and the obtained solid (referred to as RB@NaY) was dried at 60 ºC for 12 h.

2.3. Drug release studies of 5-FU@zeolites

Drug release from loaded 5-FU@zeolite samples was studied by HPLC analysis at λ = 260 nm. The simulated body fluid was made using known amounts of a buffer solution of sodium monobasic phosphate and sodium dibasic phosphate (PBS). Known amounts of the DDS were mixed (10 mg) in 50 mL of PBS solution in order to simulate body fluid at pH 7.4 and 37 °C. The samples were stirred at *ca*. 60 rpm and 5 mL aliquots of DDS/PBS were removed at regular intervals and an equal amount of fresh dissolution medium was added to keep the volume of mixture constant (50 mL). The aliquots were filtered through a 0.20 μm filter (Whatman) and analyzed by HPLC. The amount of released 5-FU was calculated using the equation previously described [36]. Experiments were conducted in triplicate and the values were averaged. The release studies were carried out for 48 h, corresponding to the time of contact of DDS with the cells.

2.4. Cell culture conditions and cell viability assays

HCT-15 and RKO were used in this study as models of human colorectal carcinoma. HCT-15 colon carcinoma cells were maintained in RPMI 1640 medium (Gibco) and RKO colon carcinoma cells were maintained in DMEM medium (Gibco). Both cell lines were supplemented with 10% (v/v) fetal bovine serum (FBS) (Gibco, Invitrogen, USA) and 1% (v/v) penicillin-streptomycin solution (P/S) (Invitrogen, USA) and incubated at 37 °C in a 5% CO_2 humidified atmosphere. Cells were subcultured approximately every three days and maintained in a log-phase growth.

Cell viability was assessed using the *In Vitro* Toxicology Assay Kit, Sulforhodamine B based (Sigma-Aldrich, St. Louis, MO, USA). HCT-15 (7500 cells/100µL/well) and RKO (6000 cells/100µL/well) cells were seeded in 96-well plates and incubated at 37 °C in a 5% CO_2 humidified atmosphere for 24 h. In order to assess the effects of the starting zeolites, 5-FU and DDS used and cells were incubated with increasing concentrations of the systems in culture medium. Controls were performed with culture medium alone. After an incubation period of 48 h, the spent media were removed and the plate wells were washed with 1x Phosphate-buffered solution, pH 7.4 (PBS). After a fixation step with cold 10% trichloroacetic acid (TCA), cells were stained with 0.4% Sulforhodamine B and the incorporated dye was solubilized with Sulforhodamine B solubilization solution (10 mM Tris). Absorbance was monitored with a microplate reader at 570 nm with a background absorbance of 655 nm. Cell viability was determined as percentage of viability: (OD experiment/OD control) x 100 (%). Results are presented as mean ± standard deviation (SD) of three independent experiments, each in triplicate. One-way ANOVA, followed by Dunnett post test (Fig. 6 and 7) were used to perform cell viability assay statistical analysis. The previous tests and 50% growth inhibition (IC_{50}) were determined using the Graphpad Prism 5® software. Values were considered statistically significant in all experiments when $p<0.05$.

2.5. Fluorescence microscopy assays

HCT-15 (10000 cells/500µL/well) and RKO (50000 cells/500µL/well) cell lines were seeded on coverslips in 24-well plates and incubated at 37 ºC in a 5% CO_2 atmosphere for 24 h. Spent media were removed, cells were washed with PBS 1x and then incubated with 0.025 mg/mL of RhodamineB@NaY during 48 h. Cells were washed twice with PBS-Tween 0.05% (PBST 0.05%), fixed with cold methanol during 10 min, washed twice with PBST 0.05% and permeabilized with PBST 0.01% for 10 min.

Next, and after two washes with PBST 0.05%, cells were blocked with FBS 10% in PBST 0.05% during 30 min and then incubated with anti-β-tubulin antibody (ab6046, Abcam®) diluted in FBS 5% in PBST 0.05% (1:700) during 1 h at room temperature. In the next step, cells were washed three times with PBST 0.05% (10 min each) and incubated with the secondary antibody anti-rabbit Alexa Fluor 488 (A11008, Invitrogen) diluted in FBS 5% in PBST 0.05% (1:1000) during 1 h at room temperature. Finally, after three washes with PBST 0.05% (10 min each) and one wash with PBS (5 min), cells were mounted in Vectashield mounting media with 4',6'-diamidino-2'-phenylindole (DAPI) (Vector Laboratories). Images were acquired in an Olympus IX81 fluorescence microscope (Tokyo, Japan), using Cell P software.

2.6. Characterization methods

The textural characterization of the zeolites was based on the N_2 adsorption isotherms, determined at -196 ºC with a Quantachrome NOVA 4200e apparatus. The samples were previously outgassed at 150 ºC under vacuum. The micropore volumes (V_{micro}) and mesopore surface areas (S_{meso}) were calculated by the t-method. Surface areas were calculated by applying the BET equation. Mesoporous size distributions were obtained from the desorption branch of the isotherm using the Barrett, Joyner and Halenda (BJH) method [37]. Elemental analyses of carbon, nitrogen, and hydrogen were carried out on a LECO CHNS-932 equipment. Scanning electron micrographs (SEM) were collected on a LEICA Cambridge S360 Scanning Microscope equipped with an EDX system for NaY and 5-FU@NaY. The

morphology of NanoNaY, 5-FU@NanoNaY, LTL and 5-FU@LTL was studied by scanning electron microscopy using a NanoSEM–FEI Nova 200 (FEG/SEM) equipped with an EDX system. In order to avoid surface charging, samples were coated with gold in vacuum prior to analysis, by using a Fisons Instruments SC502 sputter coater. ^{1}H-^{13}C cross-polarization/magic angle spinning nuclear magnetic resonance (^{13}C-CP/MAS NMR) and MAS ^{27}Al spectra were recorded on a 9.4 T wide-bore (400 MHz, ^{1}H Larmor frequency) Bruker Avance III spectrometer. A 4 mm double-resonance MAS probe was employed at 100.6 MHz (^{13}C) and 104.2 MHz (^{27}Al) Larmor frequencies. Samples were spun in ZrO_2 rotors using a spinning rate of 10 and 14 kHz, respectively for ^{13}C and ^{27}Al experiments. ^{13}C-CP/MAS NMR spectra were recorded using a ramp step (varying from 100% to 50% in amplitude using 100 points); contact time: 3.0 ms; ^{1}H 90° excitation pulse: 2.5 μs; ^{1}H and ^{13}C radio-frequency field strengths for CP were set to 87 kHz and 68 kHz, respectively; recycle delay: 5 s. TPPM-15 decoupling was employed during the signal acquisition using a 4.75 μs pulse length for the basic TPPM pulse unit along the ^{1}H channel, employing a ^{1}H radio-frequency field strength of 100 kHz. ^{27}Al spectra were recorded with an excitation pulse length of 0.7 μs (corresponding to 10º flip angle) and 1 s recycle delay. The release studies were carried out by high performance liquid chromatography (HPLC – JASCO 980-PU) using an isocratic pump and a double on line detection including an UV–vis detector and refractometer. A LiChroCart 250-4 RP-18e/5 μm column from Merck with a mobile phase contained a phosphate solution (0.01 M) in methanol/water (60/40) were used for the HPLC assays. The flow rate was 0.4 mL/min and the injection volume was 20 μL and the absorbance of 5-FU was monitored at 260 nm. Calibration curve was constructed using solutions of 5-FU with concentrations from 0.0005 mg/mL to 0.10 mg/mL. Room temperature Fourier Transform Infrared (FTIR) spectra of the samples in KBr pellets were measured using a Bomem MB104 spectrometer in the range 4000-500 cm^{-1} by averaging 20 scans at a maximum resolution of 4 cm^{-1}. The loading and the thermal stability of the samples were determined by thermogravimetric analysis in a STA 409

PC/4/H Luxx Netzsch thermal analyser. The atmosphere used was high purity air (99.99 % minimum purity) with a flow rate of 50 cm^3/min. The sample holders used were crucibles of alumina oxide, supplied by Netzsch. The samples were heated between 50 and 700 ºC at 10 ºC/min to evaluate the thermal stability.

3. Results and discussion

3.1. Loading and Physicochemical Characterization of DDS

The method for the preparation of the DDS was the adsorption of 5-FU in liquid phase within the zeolite pores and channels [30,31] and the resulting DDS were characterized by several techniques.

Loading of 5-FU into the zeolites was determined by thermogravimetric analysis (TGA). All DDS present the same weight loss in the studied temperature range. Two distinct weight changes are seen in the TGA data for pure 5-FU around 200-305 ºC and 305-410 ºC, which can be attributed to the onset of melting, followed by decomposition of the 5-FU molecule [38]. In the case of drug-loaded zeolites, the weight change is extended over the entire temperature range up to 700 ºC [39]. A small weight loss at 150 ºC was also observed in the DDS, which can be attributed to the removal of physisorbed water in the zeolite [35,36]. The TGA curve for the parent zeolites shows the same weight loss around 120 ºC. The other weight changes observed in DDS were similar to the ones of 5-FU.

Table 1 shows the 5-FU loading obtained for all prepared DDS. The drug loading studies revealed significant encapsulation efficiency for NaY followed by nanoNaY and LTL. Both nanosized zeolites, nanoNaY and LTL, show similar encapsulation efficiency, *ca.* 55 %.

Table 1- Loading of 5-FU in the DDS.

DDS	5-FU (mmol)[a]	5-FU (mmol)[b]	Yield (%)[c]
5-FU@NaY	0.99	0.72	71.3
5-FU@nanoNaY	0.99	0.55	55.6
5-FU@LTL	0.99	0.52	52.5

[a]Initial 5-FU amount in the solution; [b]5-FU loading in zeolite determined by TGA; [c]Encapsulation efficiency of 5-FU in zeolites.

NaY presents a larger micropore volume than the other zeolites, suggesting that this zeolite has a higher capacity for 5-FU loading, since it adsorbs preferentially on the micropores (see supplementary data).

The release profiles of 5-FU from zeolites, NaY, nanoNaY and LTL are shown in Fig. 1. The results were similar, with maxima of 80%, 94% and 89% 5-FU release up to 48 h for NaY, nanoNaY and LTL, respectively.

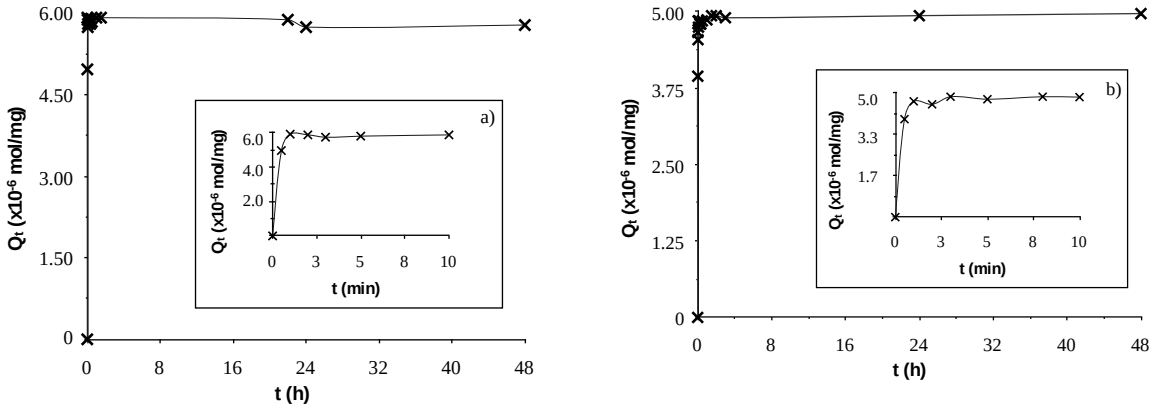

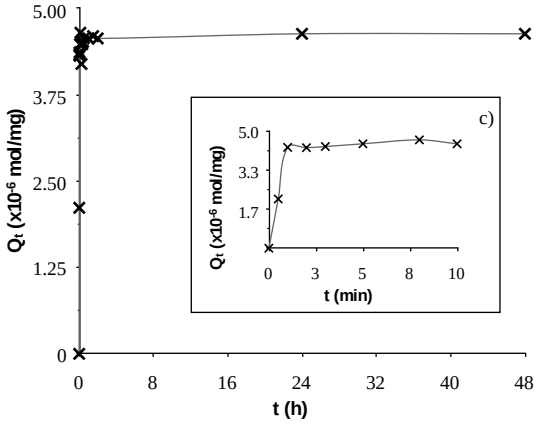

Fig. 1. Release profiles of (a) 5-FU@NaY, (b) 5-FU@nanoNaY and (c) 5-FU@LTL. The insets correspond to the 5-FU release from the DDS up to 10 min. The release was measured in a phosphate buffer solution (PBS) at pH = 7.4 and 37 ºC. $Q_t = \frac{n_{t_{corr}}}{W}$. where $n_{t_{corr}}$ [36] the number of moles at time *t* (corrected to account for changes in volume) and W is the weight (mg) of the zeolite.

All three zeolites show similar initial burst rates of 5-FU release with an exponential-type behavior and *ca.* 80-90% 5-FU release in the initial 10 min. The similarity observed in the 5-FU release profiles seems to be not dependent of the framework structure of the zeolites, 3D (Y zeolite) or 1D (LTL zeolite). The diffusion from within the zeolite pores and channels appears to be no different from the internal surface or even from the aggregate of particles.

In order to establish the best release profile, the DDS release kinetic profiles were modeled by fitting the mathematical kinetic models usually used to describe *in vitro* drug dissolution and release from pharmaceutical dosage forms [40], including the zero-order ($Q_t = Q_0 + K_0 t$), first-order ($\ln Q_t = \ln Q_0 + K_t t$), Higuchi ($Q_t = K_H \sqrt{t}$), Hixson-Crowell ($Q_0^{1/3} - Q_t^{1/3} = K_s t$), Korsmeyer-Peppas ($Q_t/Q_\infty = K_k t^n$) and Weibull ($\log[-\ln(1-(Q_t/Q_\infty))] = b\log t - \log a$) models [40]. The release models with major application and best describing drug release are the zero-order, Higuchi, Korsmeyer-Peppas and Weibull models [40,41]. The fitted data for the selected release kinetic models are listed in Table 2.

Table 2- Fitted parameters of the kinetic models used in the *in vitro* drug release of DDS.

Mathematical models	5-FU@NaY	5-FU@nanoNaY	5-FU@LTL
Zero order			
K_0 (h^{-1})	$41.5x10^{-6}$	$1.2x10^{-6}$	$2.5x10^{-6}$
R	0.4416	0.6567	0.5475
Higuchi			
K_H ($h^{-1/2}$)	$6.6x10^{-6}$	$1.2x10^{-6}$	$2.6x10^{-6}$
R	0.5943	0.7806	0.6657
Korsmeyer-Peppas			
K_p (h^{-n})	1.04	1.06	1.25
n	0.03	0.05	0.17
R	0.8361	0.9111	0.8304
Weibull			
T_i (h)	0.002	0.001	0.010
b	0.37	0.30	0.51
a	0.09	0.13	0.10
R	0.9975	0.9851	0.8988

K_0, K_H and Kp are the release rate constants; *n* is the release exponent; T_i is the time parameter (time interval necessary to release 50% to 90% of the drug); *b* is the shape parameter and *a* is the scale parameter.

The *in vitro* drug release from zeolites was best described by the Weibull model, as the plots showed the highest linearity. The Weibull model is more useful for comparing the release profiles of matrix-type drug delivery [41]. This model describes the dissolution curve in terms of applicable parameters and is able to empirically describe, but not mechanistically characterize, the dissolution behavior of the dosage form. The advantage of the Weibull model lies on its ability to fit almost any kind of dissolution curve and it is, therefore, often used to describe experimental data, especially when the mechanism of release underlying the dissolution behavior is unknown [42]. In this model, the shape parameter, *b*, characterizes the

curve as exponential (b=1, case 1), sigmoid, S-shaped, with upward curvature followed by a turning point (b>1, case 2), or parabolic, with a higher initial slope and after that consistent with the exponential (b<1, case 3) [40-42]. The b parameter obtained after fitting the release data was 0.37, 0.30 and 0.51 for 5-FU@NaY, 5-FU@nanoNaY and 5-FU@LTL, respectively. These values are consistent with case 3 exhibiting higher initial slope followed by an exponential curvature, as it is evident from the release profiles for all DDS in Fig. 1.

The rapid release of 5-FU from zeolites may be rationalized in terms of the size of the drug and its interactions with the zeolite frameworks. 5-FU is a small molecule with molecular dimensions 4.936 Å x 5.387 Å x 5.043 Å, which can easily diffuse out of the micropores of faujasite and Linde type L. These zeolite structures have similar pore opening diameters, which results in the enhanced release of the drug in the buffer solution.

The ^{13}C NMR spectrum of 5-FU shows the characteristic peaks of the drug molecule with resonances at δ_{13C} = 161.6 (C4), 149.5 (C2), 139.3 (C5) and 130.0 (C6) ppm, consistent with previous assignments [43]. The presence of the 5-FU C2, C5 and C6 peaks in the ^{13}C CP/MAS spectrum of 5FU@NaY indicates both, the presence and integrity of the drug, and minimal interactions with the zeolite framework (see supplementary data). The poor signal-to-noise ratio of this spectrum (despite 22 h of acquisition) does not allow confirmation of the presence of the C4 resonance, whose observation may also be hindered by longer ^{1}H relaxation. ^{27}Al solid-state MAS NMR spectra of all samples are identical showing that the experimental procedure used does not damage the structure of the zeolites and providing no evidence for significant framework-drug interactions.

Fourier Transformed Infrared spectroscopy (FTIR) also does not reveal any significant interactions between the drug and the zeolite (see supplementary data). The 5-FU spectrum shows the characteristic vibrational modes of the anticancer molecule. The bands at 1722, 1660 and 1246 cm^{-1} are attributed to the cyclic imide, CO-NH-CO. The bands at 1430 cm^{-1} are attributed to C–H stretching in –CF=CH– and the C–H deformation vibration band in –

CF=CH– is observed at 814 cm^{-1} [4,7,44]. In the region 2750-3200 cm^{-1}, the vibrational stretching modes from C–H and N–H were also observed [7].

For the prepared DDS, the FTIR spectra are dominated by the strong bands assigned to the vibrational modes arising from the zeolite structure. The presence of physisorbed water is detected by the ν(O-H) stretching vibration at 3410 cm^{-1} and the ν(O-H) deformation band at 1635 cm^{-1}. The bands corresponding to the lattice vibrations are observed in the spectral region between 1300 and 450 cm^{-1} [25,31]. No shift or broadening in the principal zeolite vibrational bands occur upon inclusion of the drug, further substantiating that the zeolite frameworks remain unchanged. The spectra of the DDS display the bands attributed to 5-FU, with no measurable shifts indicating that the drug is present and not interacting strongly with the zeolitic frameworks.

3.2- Drug bioactivity studies

The cytotoxicity studies were carried out in two different cancer cell lines, HCT-15 and RKO. These lines are well characterized human colorectal carcinoma cells, with different phenotypes and genetic backgrounds. These cells were chosen as predictive models to test the potentiation of the chemotherapeutic agent 5-FU into the zeolites NaY, nanoNaY and LTL. Viability of HCT-15 and RKO cells was evaluated by the sulforhodamine B (SRB) assay, which measures the drug-induced cytotoxicity and cell proliferation, used for large-scale drug-screening applications [45].

The drug bioactivity studies were performed by preparing five working DDS concentrations, by diluting a stock suspension (1.0 mg/mL) in culture medium. For better homogenization, all suspensions were submitted to ultrasonic dispersion for 2 min prior to use. This procedure was optimized in our previous work [31].

The cytotoxicity of the starting zeolites, NaY, nanoNaY and LTL, was investigated in HCT-15 and RKO cell lines to assess their suitability as DDS. In both cell lines, all zeolites gave

similar results according to our previous work, showing no significant toxicity [31]. Fig. 2 and 3 show the effects on cell viability obtained when treating HCT-15 and RKO cells with the non-encapsulated 5-FU and 5-FU@zeolite systems, when taking into consideration the amount of drug present in the DDS systems for the different suspensions used.

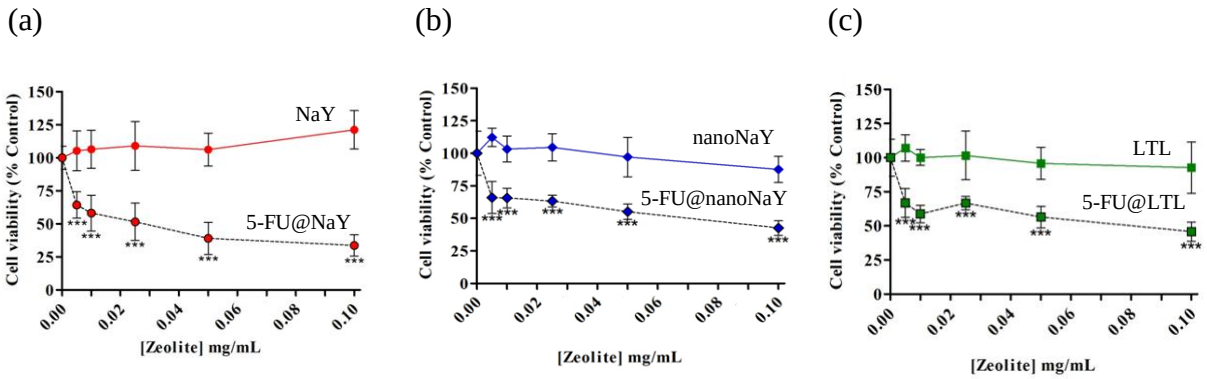

Fig. 2. Effect of NaY (a), nanoNaY (b) and LTL (c) zeolites and DDS systems on HCT-15 colon carcinoma cell viability. HCT-15 cell line was incubated with zeolites and different DDS concentrations for 48 h. Cell viability was measured by SRB assay. Values are means ± SD of three independent experiments, each performed in triplicate. ***p<0.001 compared to zeolite alone.

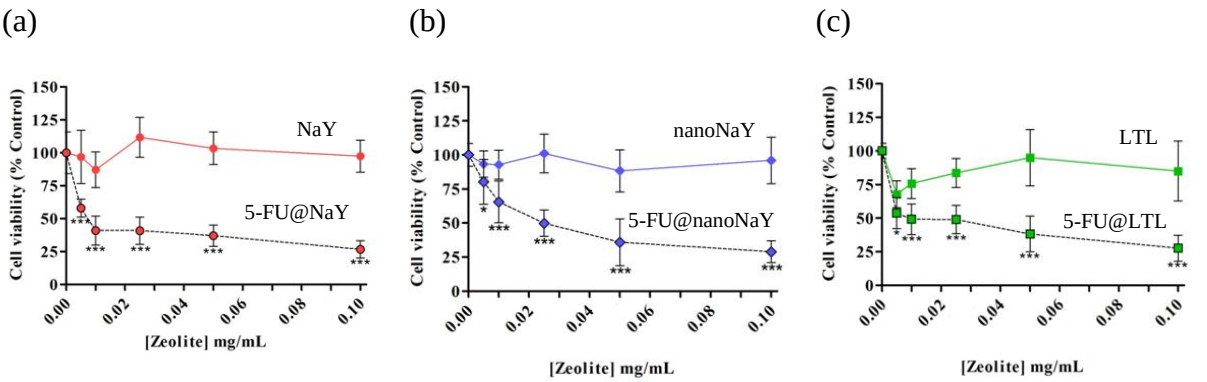

Fig. 3. Effect of NaY (a), nanoNaY (b) and LTL (c) zeolites and DDS systems on RKO colon carcinoma cell viability. RKO cell line was incubated with zeolites and different DDS concentrations for 48 h. Cell viability was measured by SRB assay. Values are means

± SD of three independent experiments, each performed in triplicate. *p<0.05, ***p<0.001 compared to zeolite alone.

The differences between controls (without zeolite) and the range of zeolite concentrations are non-significant, showing in this way that all zeolites are non-toxic to the cells for the selected period of incubation and concentrations. Compared to zeolites alone (control), there is an evident reduction in cell viability, with increasing concentrations of 5-FU in the zeolite system for both cell lines. For HCT-15 cell line, 5-FU encapsulated into NaY, nanoNaY and LTL, led to a reduction in cell viability from 64 to 34%, 66 to 43% and 67 to 46% comparing with cells treated with the starting zeolite. In RKO cells (Fig. 3), incubation of the 5-FU@zeolite systems resulted also in a significant decrease in cell viability for the three zeolite systems: from 58 to 27% for 5-FU@NaY, 80 to 29% for 5-FU@nanoNaY and 54 to 28% for 5-FU encapsulated in LTL zeolite. Moreover, the reduction in viability was more pronounced in RKO cell line.

5-FU working concentrations (0.01, 0.10, 1 and 10 mM) were obtained by diluting the stock solution (1 M) in culture medium. It is possible to observe a dose-dependent decrease in cell viability, being the IC_{50} values of 0.61 mM for HCT-15 cells and 0.13 mM for RKO (Table 3).

Table 3- 5-FU, 5-FU@NaY, 5-FU@nanoNaY and 5-FU@LTL IC_{50} values for HCT-15 and RKO cell lines.

	HCT-15		RKO	
	IC_{50} (mM)	Potentiation	IC_{50} (mM)	Potentiation
5-FU	0.61	--	0.13	--
5-FU@NaY	0.08	7.6	0.03	4.3
5-FU@nanoNaY	0.21	2.9	0.08	1.6
5-FU@LTL	0.31	1.9	0.03	4.3

By comparing the results obtained when treating cells with the non-encapsulated 5-FU with the encapsulated 5-FU, there is an obvious potentiation of the effect of the drug. For HCT-15, there is an increase in efficiency of the drug between 1.9 and 7.6-fold, corresponding to 5-FU assay concentrations of 0.08 and 0.31 mM, respectively. Likewise, treatment of RKO cells with the encapsulated 5-FU resulted in a potentiation of the effect of the drug from 1.6 to 4.3 fold.

For HCT-15 cells, NaY DDS was more effective than the two remaining nanosized DDS, probably due to the higher 5-FU loading in zeolite Y. For RKO cells, both NaY and LTL DDS show the same potentiation. In this case, particle size could have justified the similar potentiation. However, the different potentiation obtained with LTL in the two cell lines is not clear, warranting further studies. For higher concentrations of the DDS or starting zeolites (above 0.25 mg/mL), cell viability began to be affected, likely due to the compromise of cell-nutrient exchange with the culture media [30,31].

In order to assess the interaction between the zeolites and the CRC cells, fluorescence microscopy assays were performed. Fig. 4 shows the results where HCT-15 and RKO cells were treated with the NaY zeolite loaded with the fluorescent compound Rhodamine B.

Comparing the control images with those with RhodamineB@NaY, it is possible to observe that the zeolite is able to enter the cell cytoplasm. Although this approach was only applied to NaY zeolite, it is expected that both nanoNaY and LTL zeolites are also able to enter the cells due to their smaller dimensions, where internalization would be even easier. Extrapolating these results for the DDS, it is likely that the drug release is achieved inside the cells if the DDS is put in contact with them.

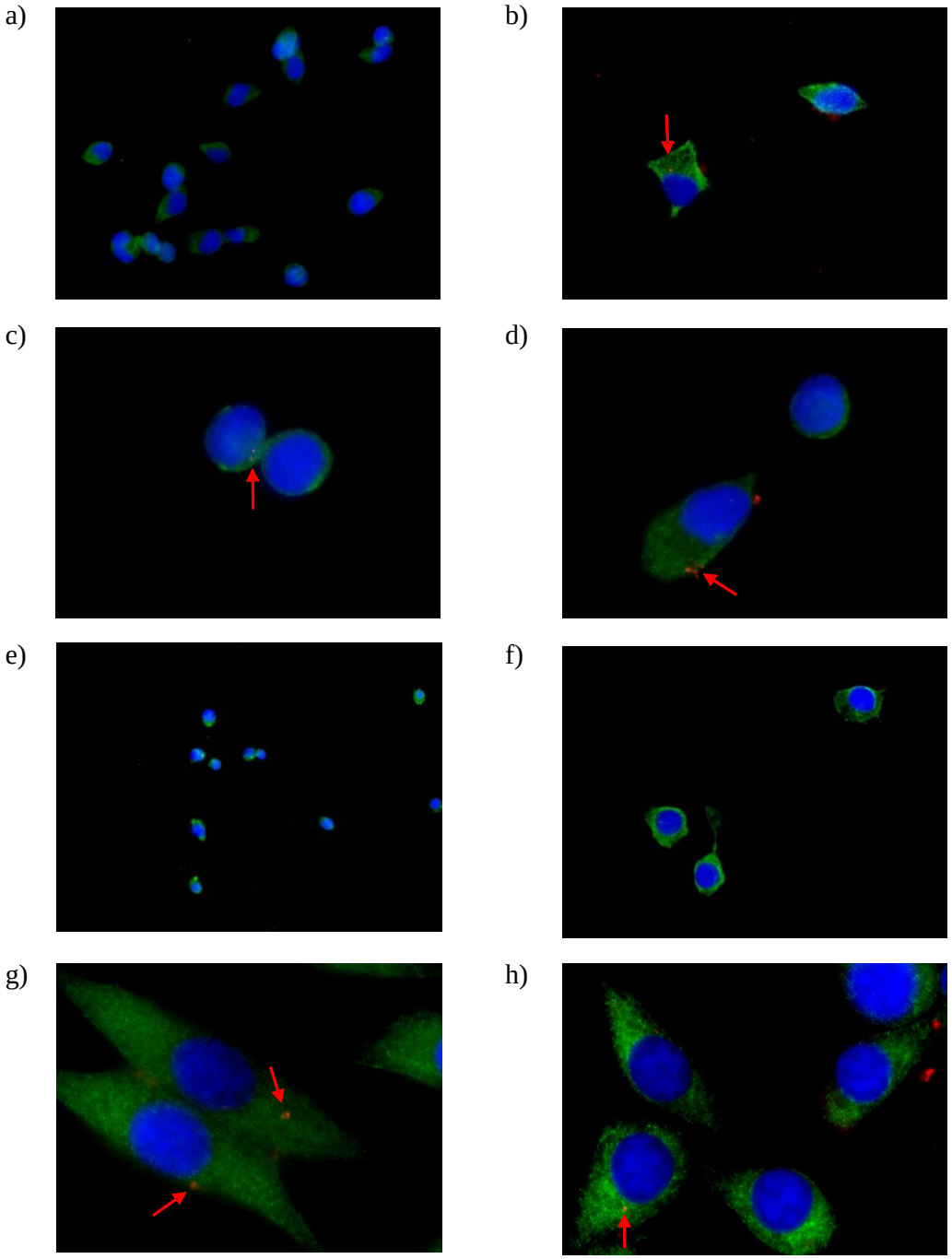

383

384

385 **Fig. 4.** Fluorescence microscopy images showing the cellular localization of NaY zeolite
386 loaded with Rhodamine B in CRC cell lines (red, arrows). HCT-15 cell line: (a)-(d);
387 RKO cell line: (e)-(h); Control: (a), (e) and (f); RB@NaY: (b), (c), (d), (g) and (h).
388 Nucleus/DAPI (blue), β-tubulin/FITC (green), RB@NaY/TRITC (red); 200x (e); 400x
389 (a) and (f); 600x (b); 1000x (c), (d), (g) and (h).

By encapsulating 5-FU into zeolites, we increased significantly the efficiency of this drug. We believe that similarly to other systems [16, 46-48], the zeolite DDS allow the release of 5-FU, increasing the bioavailability of the drug, and thus explaining the increase in potency. Moreover, the entry of 5-FU into the cells could also contribute to the high increase in potency observed. Thus, this potency rise could be the combined result of both the increase in 5-FU bioavailability and the facilitation of 5-FU entry into the cell by the DDS.

4- Conclusions

5-FU was successfully loaded into the zeolite structures with different particle sizes, NaY (700 nm) and two nanosized zeolites, nanoNaY (150 nm) and nanoLTL (80 nm) and the loading of 5-FU was found to be highest in NaY followed by nanoNaY and LTL. FTIR and solid-state NMR (^{13}C and ^{27}Al) provided no evidence for significant framework-drug interactions. The release of the drug from the zeolite structures in buffer solution at pH = 7.4 and 37 °C followed the Weibull model. The effect of the zeolites and DDS on HCT-15 and RKO human colon carcinoma cell lines viability was evaluated. DDS based on zeolites were able to increase the efficiency of 5-FU, a widely used anticancer drug. We believe these systems should be further explored in other cancer models, e.g. *in vivo* models, to confirm the efficiency of the systems.

Acknowledgments

RA is recipient of fellowship SFRH/BI/51118/2010 from Fundação para a Ciência e a Tecnologia (FCT, Portugal). This work was supported by the FCT projects refs. PEst-C/QUI/UI0686/2011 and PEst-C/CTM/LA0011/2011 and the Centre of Chemistry and Life and Health Sciences Research Institute (University of Minho, Portugal). The NMR

spectrometer is part of the National NMR Network (RNRMN), supported with funds from FCT/QREN (Quadro de Referência Estratégico Nacional).

References

[1] A. Jemal, R. Siegel, E. Ward, Y. Hao, J. Xu, T. Murray, M.J. Thun, CA Cancer J. Clin. 58 (2008) 71-96.

[2] T. Ishikawa, M. Utoh, N. Sawada, M. Nishida, Y. Fukase, F. Sekigochi, H. Ishitsuka, Biochem. Pharmacol. 55 (1998) 1091-1097.

[3] N.J. Meropol, Eur. J. Cancer 34 (1998) 1509-1513.

[4] F.H. Lin, Y.H. Lee, C.H. Jian, J.-M. Wong, M.-J. Shieh, C.-Y. Wang, Biomaterials 23 (2002) 1981-1987.

[5] C. Heidelberger, N. K. Chaudhuri, P. Danneberg, D. Mooren, L. Griesbach, R, Duschinsky, R. J. Schnitzer, E. Pleven, J. Scheiner, Nature 179 (1957) 663-666.

[6] T. A. Rich, R. C. Shepard, S. T. Mosley, J. Clin. Oncol. 22(11) (2004) 2214-32.

[7] X. Wang, J. Lin, X. Zhang, Q. Liu, Q. Xu, R.-X. Tan, Z. Guo, J. Inorg. Biochem. 94 (2003) 186-192.

[8] F. Ciardiello, G. Tortor, Eur. J. Cancer 39 (2003) 1348-1354.

[9] F. Kabbinavar, J. Schulz, M. McCleod, T. Pattel, J. Hamm, J. R. Hecht, R. Mass, B. Perrou, B. Nelson, W. F. Novotny, J. Clin. Oncol. 23 (2005) 3697-3705.

[10] B. J. Giantonio, Nat. Rev. Clin. Oncol. 6 (2009) 311-312.

[11] D. Odom, B. Barber, L. Bennett, M. Peeters, Z. Y. Zhao, J. Kaye, M. Wolf, J. Wiezorek, Int. J. Colorectal Dis. 26(2) (2011) 173-181.

[12] R. F. Ozols, R. S. Herbst, Y. L. Colson, J. Gralow, J. Bonner, W. J. Curran, B. L. Eisenberg, P. A. Ganz, B. S. Kramer, M. G. Kris, M. Markman, R. Mayer, D. Raghavan, G. H. Reaman, R. Sawaya, R. L. Schilsky, L. M. Schuchter, J. W. Sweetenham, L. T. Vahdat, R. J. Winn, J. Clin. Oncol. 25 (2007) 146-162.

[13] C. M. Walko, C. Lindley, Clin. Ther. 27(1) (2005) 23-44.

441 [14] S. Farquharson, A. Gift, C. Shende, F. Inscore, B. Ordway, C. Farquharson, J. Murren,
442 Molecules 13 (2008) 2608-2627.
443 [15] J.L. Arias, Molecules 13 (2008) 2340-2369.
444 [16] Y. Zhu, T. Ikoma, N. Hanagata, S. Kaskel, Small. 6 (2010) 471-478.
445 [17] M. Danilczuk, K. Dugopolska, T. Ruman, D. Pogocki, Mini-Rev. Med. Chem. 8 (2008)
446 1407-1417.
447 [18] D. G. Fatouros, D. Douroumis, V. Nikolakis, S. Ntais, A. M. Moschovi, V. Trivedi, B.
448 Khima, M. Roldo, H. Nazar, P. A. Cox, J. Mater. Chem. 21 (2011) 7789-7794.
449 [19] Y.H. Zhang, X.J. Yu, X. . Wang, W. Shan, P.Y. Yang, Y. Tang, Chem. Commun. (2004)
450 2882-2883.
451 [20] A. Corma, V. Fornes, F. Rey, Adv. Mater. 14 (2002) 71-74.
452 [21] C. Platas-Iglesias, L. Van der Elst, W.Z. Zhou, R.N. Muller, C.F.G.C. Geraldes, T.
453 Maschmeyer, J.A. Peters, Chem. A Eur. J. 8 (2002) 5121-5131.
454 [22] M. Norek, I.C. Neves, J.A. Peters, Inorg. Chem. 46 (2007) 6190-6196.
455 [23] M. Arruebo, R. Fernandez-Pacheco, S. Irusta, J. Arbiol, M. R. Ibarra, J. Santamaria,
456 Nanotechnol. 17 (2006) 4057-4064.
457 [24] M.G. Rimoli, M.R. Rabaioli, D. Melisi, A. Cucio, S. Mondello, R. Mirabelli, E.
458 Sbignete, J. Biomed. Mater. Res. A. 87A (2008) 156-164.
459 [25] M.M. Tsotsalas, K. Kopka, G. Luppi, S. Wagner, M.P. Law, M. Schafers, L. De Cola,
460 ACS Nano 4 (2010) 342-348.
461 [26] N. Ndiege, R. Raidoo, M. K. Schultz, S. Larsen, Langmuir 27 (2011) 2904-2909.
462 [27] A. Martucci, L. Pasti, N. Marchetti, A. Cavazzini, F. Dondi, A. Alberti, Micropor.
463 Mesopor. Mater. 148 (2012) 174-183.
464 [28] T. Ceyhan, M. Tatlier, H. Akcakaya, J. Mater. Sci. Mater. Med. 18 (2007) 1557-1562.
465 [29] A. Corma, H. Garcia, Eur. J. Inorg. Chem. 6 (2004) 1143-1164.

[30] N. Vilaca, R. Amorim, O. Martinho, R. M. Reis, F. Baltazar, A. F. Fonseca, I.C. Neves, J. Mater. Sci. 46 (2011) 7511-7516.

[31] R. Amorim, N. Vilaca, O. Martinho, R. M. Reis, M. Sardo, J. Rocha, F. Baltazar, A. F. Fonseca, I.C. Neves, J. Phys. Chem. C. 116 (2012) 25642-25650.

[32] G. Calzaferri, S. Huber, H. Maas, C. Minkow, Angew. Chem., Int. Ed. 42 (2003) 3732–3758.

[33] L. Ferreira, A. M. Fonseca, G. Botelho, C. Almeida-Aguiar, I. C. Neves, Micropor. Mesopor. Mater. 160 (2012) 126–132.

[34] I. Kuzniarska-Biernacka, K. Biernacki, A.L. Magalhães, A.M. Fonseca, I.C. Neves, J. Catal. 278 (2011) 102-110.

[35] I.C. Neves, C. Cunha, M.R. Pereira, M.F.R. Pereira, A.M. Fonseca, J. Phys. Chem. C 114(24) (2010) 10719-10724.

[36] A. Datt, D. Fields, S.C. Larsen, J. Phys. Chem. C. 116 (2012) 21382-21390.

[37] S.J. Gregg, K.S.W. Sing, Adsorption, Surface Area and Porosity, Academic Press, San Diego, 1982.

[38] R.J. Lewis, Hawley's Condensed Chemical Dictionary, 14th Edition, John Wiley & Sons, Inc. New York, NY, 2001 (page 507).

[39] A. Datt, E.A. Burns, N.A. Dhuna, S.C. Larsen, Micropor. Mesopor. Mater. 167 (2013) 182-187.

[40] P. Costa, J.M.S. Lobo, Eur. J. Pharm. Sci. 13 (2001) 123-133.

[41] S. Dash, P.N. Murthy, L. Nath, P, Acta Pol. Pharm. - Drug Research 67(3) (2010) 217-233.

[42] K. Thelen, K. Coboeken, S. Willmann, J.B. Dressman, J. Lippert, J. Pharm. Sci. 101(3) (2012) 1267-1280.

[43] F.G. Vogt, J.A. Vena, M. Chavda, J.S. Clawson, M. Strohmeier, M.E. Barnett, J. Mol. Struct. 932 (2009) 16–30.

[44] L. Huang, W. Sui, Y. Wang, Q. Jiao, Carbohyd. Polym. 80 (2010) 168–173.

[45] W. Voigt, Sulforhodamine B Assay and Chemosensitivity, in: Methods in Molecular Medicine, vol. 110: Chemosensitivity: Vol. 1: In Vitro Assays, Edited by: R. D. Blumenthal © Humana Press Inc., Totowa, NJ, 2005 (page 39).

[46] E. Gultepe, D. Nagesha, S. Sridhar, M. Amiji, Adv. Drug Delivery Rev. 62 (2010) 305-315.

[47] E. J. Anglin, L. Cheng, W. R. Freeman, M. J. Sailor, Adv. Drug Delivery Rev. 60 (2008) 1266-1277.

[48] J. L. Vivero-Escoto, I. I. Slowing, B. G. Trewyn, V. S. Y. Lin, Small 6 (2010) 1952-1967.